# COMBUSTION REGIME IDENTIFICATION ON A BLUFF-BODY BURNER BY USING EXPERIMENTAL *PLIF-OH* IMAGES AND *RANS* NUMERICAL SIMULATIONS

**Nattan Roberto Caetano**
**Americo Barbosa da Cunha Junior**
**André Reinaldo Novgorodcev Júnior**
**Luís Fernando Figueira da Silva**
Departamento de Engenharia Mecânica
Pontifícia Universidade Católica do Rio de Janeiro — PUC–Rio
Rua Marquês de São Vicente, 225, Gávea - Rio de Janeiro, RJ - Brasil - 22453-900
nattan@puc-rio.br — americo.cunhajr@gmail.com — andre9@gmail.com — luisfer@esp.puc-rio.br

***Abstract.***
*The aim of this work is to determine the different combustion regimes in a classical turbulent combustion diagram (Reynolds vs Damköhler), in order to qualify the turbulent flames that are obtained at the bluff-body experimental apparatus of the Combustion and Turbulence Laboratory at PUC–Rio. Additionally, the purpose is to estimate the influence of different fuel types (e.g. natural gas and hydrogen) on the combustion regimes. The velocity of the fuel (oxidizer) stream was varied between* 0.4 *and* 50.0 *m/s (*1.2 *and* 11.7 *m/s) in order to get representative experimental results for each flame regime within the diagram. Instantaneous and time-averaged flames thickness were obtained from the images captured via Planar Laser induced Fluorescence of the Hydroxyl Radical (PLIF-OH). Reynolds Averaged Navier Stokes (RANS) models were employed to determine the turbulence characteristics of the flow field, in terms of the dimensionless Reynolds and Damköhler numbers. The determination of the Damköhler number also required the construction of specific flamelets libraries. The experiment allowed to investigate several combustion regimes, including the laminar flame regime, the flamelet regime and the unsteady effects regime, each of which was obtained for a large range of Reynolds and Damköhler numbers. The comparison of the combustion regimes actually obtained experimentally with those estimated by using the classical regime diagram evidences the shortcomings of such a simplified approach.*

***Keywords:*** *turbulent combustion, nonpremixed combustion, CFD, PLIF-OH images, bluff-body burner*

## 1. INTRODUCTION

Bluff-body burners for nonpremixed reactants have been studied thoroughly during the past 30 years. This burner is also widely used in industrial applications, since it presents particular features that enhance the fuel oxidizer mixture, excellent flame stability and easy combustion control. Indeed, the bluff-body stabilizes the flame by the intense fuel/air mixing and by the presence of burned gases which provide a continue ignition source in the re-circulation zone. Bluff-body stabilized flames have received significant attention during the past few years due to their relevance to different engineering applications interesting in industrial problems and were studied experimentally and numerically in several works, e.g., Dally et al. (2003) and Merci et al. (2001). A review work about bluff-body stabilized combustion was performed by Dally et al. (1998). Essentially, the obtained experimental data has been compared to presumed probability density function (PDF) calculations of mean mixture fraction and of the RMS of the mixture fraction fields, under the hypothesis that the flames investigated are stochastically axisymmetric. This kind of burner is able to support flames within a complex recirculation zone, also allowing for regimes which span from the laminar to the turbulents ones. This emphasizes the existence of a controlled flow media where the interaction between turbulence and chemical kinetics can be investigated. Furthermore, the bluff-body provides broad optical access to apply measurements based on laser techniques in combustion diagnostics. This burner provides a broad test range for chemical models and turbulence, as well as the symmetrical arrangement suitable for computational modelling. Due to the simple and well defined initial and boundary conditions, the bluff-body burner is a prospective subject of studies of the poorly known turbulence and chemical interactions that occur in turbulent recirculating flows. This burner also has the capacity of keeping the stabilized flames in a large range of flow conditions.

Although the practical and theoretical importance of the bluff-body burner in the study of combustion is clearly established, to the best of the authors knowledge, there is no work in the literature which classifies the flame regimes according to the classical Damköhler versus Reynolds nonpremixed combustion diagram, Poinsot and Veynante (2005). The aim of this work is to provide an understanding of the stability and of the flame

structure in a bluff-body burner. Thus, this study focus on Reynolds and Damköhler influence analysis for several turbulent combustion regimes of the nonpremixed natural gas (methane) or hydrogen flames reacting on coflow with air. A comparison between numerical model and experimental results allows to identify different combustion regimes. The experimental results were obtained using laser induced fluorescence (LIF) to characterize the $OH$ radical distribution. The modelling approach combines a nonreactive computational fluid dynamics characterization of the flow-field together with a chemical time scale estimate using a detailed description of the chemical kinetics. This evaluation is performed with the aim of developing a better knowledge about the combustion regimes that could be found on the burner. Thus, the nonpremixed turbulent flame structure study allows to identify the occurrence and the influence on the flame structure of main control parameters, i.e., the Damköhler and Reynolds numbers, on the combustion regimes which could be obtained. The obtained results may be used to guide the choice of turbulence and combustion models to describe the resulting flow structures.

## 2. NONPREMIXED COMBUSTION REGIMES

The turbulent nonpremixed combustion regimes can be identified by comparing characteristic flame scales to characteristic turbulent scales, Poinsot and Veynante (2005). In this work the nonpremixed combustion regimes will be described based on the turbulent Reynolds number and on the Damköhler number and organized according to the classical diagram shown in Figure 1.

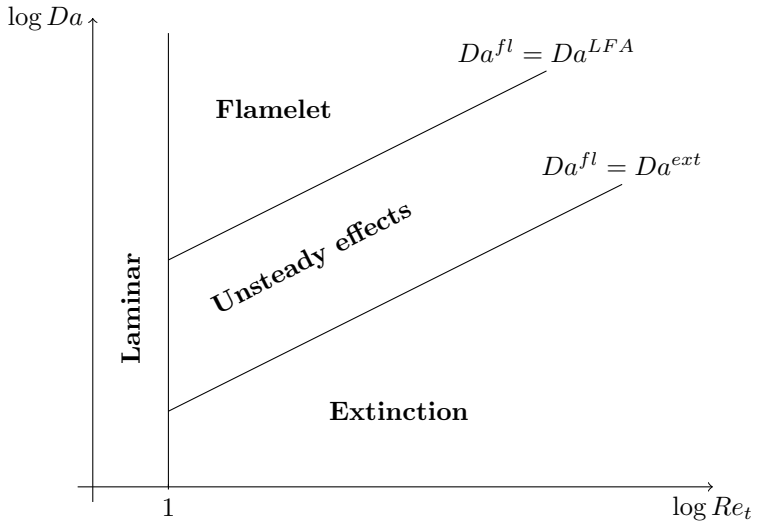


Figure 1. Regimes for turbulent nonpremixed combustion as a function of the Damköhler number, $Da$, and the turbulent Reynolds numbers $Re_t$, Poinsot and Veynante (2005).

The turbulent Reynolds number is defined as

$$Re_t = \frac{\kappa^2}{\nu\varepsilon}, \tag{1}$$

where $k$ is turbulent kinetic energy, $\varepsilon$ is the turbulent kinetic energy dissipation rate and $\nu$ is kinematic viscosity. As described in the following section, the turbulent Reynolds number was estimated using the results from the numerical simulations of the flow field aerodynamics.

The turbulent Damköhler number is defined as

$$Da = \frac{\tau_t}{\tau_c} = \frac{N}{\omega}, \tag{2}$$

where $\tau_t$ is a turbulence characteristic integral time, $\tau_c$ is a timescale from the chemical reaction, $N$ is the scalar dissipation rate, which corresponds to a laminar flamelet extinction, and $\omega$ is the turbulence eddy frequency.

Even if the premixed flame structure can be characterized by the Damköhler number, $Da$, this dimensionless group is of lesser relevance for the nonpremixed local flame structure, which is characterized by the local

Damköhler number

$$Da^{fl} = \frac{\tau_f}{\tau_c}, \tag{3}$$

where $\tau_f$ is a local flow timescale which is obtained from the CFD simulations. Its possible to show, (Poinsot and Veynante, 2005, section 6.3.3), that

$$Da \approx 2\sqrt{Re_t} Da^{fl}. \tag{4}$$

For infinitely fast chemistry, i.e., small values of $\tau_c$ and, thus for large values for $Da$, the flame is very thin and may be identified to a laminar flame element (flamelet). For larger values of $\tau_c$ the thickness of the reactive layer becomes of the same order as the Kolmogorov scale, so the fast chemistry hypothesis is no longer valid and unsteady and turbulence effects are expected. For even lower Damköhler numbers, extinctions may occur, Poinsot and Veynante (2005).

Constant values for $Da^{fl}$ correspond to lines with slope of 1/2 in the diagram shown in Figure 1. For sufficiently fast chemistry, the flame is supposed to be composed of laminar flame elements (flamelets), $Da^{fl} \geq Da^{LFA}$. Extinction should occur for large chemical times, which may be written as $Da^{fl} \leq Da^{ext}$.

## 3. METHODOLOGY

The nonpremixed turbulent flames studied are stabilized at the bluff-body burner of the Combustion and Turbulence Laboratory of the Mechanical Engineering Department at the Pontifícia Universidade Católica do Rio de Janeiro — PUC–Rio. A complete description of the experimental setup and used equipments is available at the works of Alvarez Aquino (2006), Alvarez Aquino et al. (2007) and Alva (2008). These flames are studied experimentally and numerically, using two different fuels (natural gas and hydrogen), reacting with coflow air at ambient conditions. The fuel feed diameter is 7.1 $mm$, the bluff-body base diameter is 60 $mm$ and the air coflow diameter is 200 $mm$. A scheme of the experimental apparatus is presented in the Figure 2.

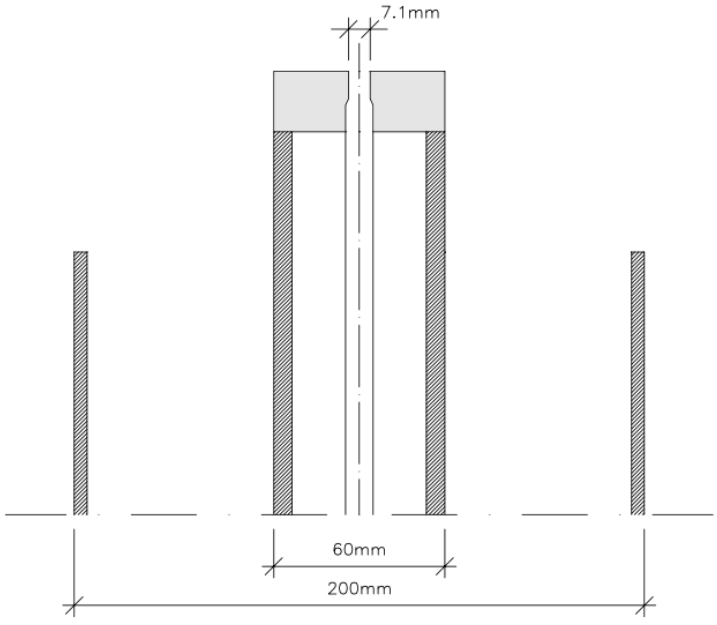


Figure 2. Sketch of the bluff-body burner.

### 3.1 Numerical Approach

The numerical model consists of an axisymmetric geometrical configuration for the bluff-body similar to that used by Alva (2008) and Alva et al. (2008). Statistically stationary flow regime is assumed and the turbulent transport in the flow is modelled using a Reynolds Average Navier Stokes (RANS) model, namely the standard $k-\epsilon$ model by Jones and Launder (1972). The $k-\epsilon$ model is used to determine the turbulent kinetic energy and

the turbulent eddy frequency of the fluid flow which are used for constructing an *a priori* combustion regime diagram. The complete description of the numerical modelling can be found in Alva et al. (2008) and Alva (2008).

In this work, the fuel jet and coflow velocities are varied, following the values shown in Table 1, in order to investigate the effect of the Reynolds and Damköhler numbers on the resulting nonpremixed turbulent combustion regimes. For each of these flow conditions, a solution of the nonreactive flow field is obtained on a computational domain and corresponding to a mesh which has been shown to lead to mesh independent flow properties, Lemay et al. (2008). Even if the $k-\epsilon$ model is know to provide only an approximate description of the Reynolds stresses on such flow field, when compared to more elaborate Reynolds stress transport models, it is deemed sufficient to the present purpose of providing an *a priori* estimate of the flow properties. Once a solution is obtained, the region at vicinity of the bluff-body, that spans 1.5 diameters above and 1.0 diameters along it, is divided in 25 equally distributed volumes and the averaged turbulent frequency and Reynolds number are determined by arithmetic average of the computational cells encompassed by each volume. These average values are then employed to construct the *a priori* combustion diagrams. All simulations of the flow field hydrodynamics reported in this section were performed with the CFD package ANSYS CFX.

Table 1. Typical fuel and air velocities used at the bluff-body experimental apparatus, Alva (2008).

| $U_{fuel}$ $(m/s)$ | $U_{air}$ $(m/s)$ |
|---|---|
| 1.3 | 1.2 |
| 2.2 | 1.2 |
| 2.9 | 1.2 |
| 6.9 | 1.2 |
| 1.3 | 6.6 |
| 2.2 | 6.6 |
| 2.9 | 6.6 |
| 6.9 | 6.6 |
| 2.2 | 11.7 |
| 2.9 | 11.7 |
| 6.9 | 11.7 |

The calculation of the Damköhler number requires the modelling of the reaction zone characteristics, and, in particular, of a chemical time scale. A modified version of the OPPDIF code by Lutz et al. (1996) was used with CHEMKIN-II package Kee et al. (1989) to generate flamelet libraries for the different fuels at 294 $K$. The detailed chemical mechanism of the Gas Research Institute, Bowman et al. (1998), was used to describe methane kinetics, whereas the mechanism proposed by Li et al. (2004) describes the thermochemical evolution of hydrogen air mixtures. Each flamelet library describe how the thermochemical properties of the instantaneous flame element, i.e., temperature and species mass fractions, evolves in mixture fraction, $Z$, space for different values of the scalar dissipation rate, $N$, ranging from equilibrium to extinction conditions. These flamelet libraries were used to obtain the values of the chemical timescale, which is the inverse of the critical value of the scalar dissipation rate above which combustion is extinguished. In cases where the reaction rate is lower than the passive scalar mixing rate, the flamelet Damköhler number is smaller than unity, and vice-versa. Combining the CFD and the detailed chemistry approach allows one to build an *a priori* combustion regime diagram.

### 3.2 Experimental Approach

The burner system was designed to produce several regimes of turbulence combustion interactions representative of practical applications. The fuel is delivered to the burner by a 7.1 $mm$ diameter orifice. The fuel flow is measured on the OMEL flowmeter, model 3P5-0401V01, which has a nominal flow rate of 3.3 $Nm^3/h$, which limits the maximum power of the apparatus in 33 $kW$ (for natural gas). Air is supplied to the burner via a centrifugal fan with nominal power and volume flow rate of 4 $CV$ and 0.55 $Nm^3/s$. The minimal air coflow velocity achieved by this system is 1.2 $m/s$ and maximal is 11.7 $m/s$, respectively for the rotational frequencies of the 20 $Hz$ and 60 $Hz$.

The combustion diagnostic laser system is composed by a pump laser, a dye laser and a optical system which generates a laser light sheet used to excite the $OH$ molecules whose fluorescence is to be measured. The measurements of the hydroxyl radical fluorescence is performed assuming that this species is presumed to

play the role of the flame front tracer Wolfrum (1998). A Quantel solid state Nd:YAG pumped laser, model Brilliant b, 5 $ns$ pulse width, yields 2.6 $W$ at 10 $Hz$ and 355 $nm$ wavelength. The pulsed beam is guided by mirrors to a Sirah dye laser, model CSTR-G-3000 whose tuning is granted at the excitation wavelength with a picometer precision. The dye used to induce the OH fluorescence is the Coumarin-153 dissolved on ethanol at 1.6 $kg/m^3$ concentration, yielding 15% of the maximum efficiency at the bandwidth 517 $nm$ to 574 $nm$. Prior to the test section the laser beam is frequency doubled by a BBO crystal, in order to obtain of a wavelength of about 283 $nm$ with 25 $mW$ average output power. A 0.5 $mm$ thickness laser light sheet is formed after passing through a spherical lens system. In order to obtain a quantitative value of $OH$ fluorescence intensity Petersson et al. (2007) suggest the Q1(8) transition line, which is relatively temperature insensible. The chosen excitation wavelength is thus 283.561 $nm$ relative to the rotational $\nu' = 0$ and vibrational $\nu'' = 1$ states of the A-X (1,1) e (0,0) system, and fluorescence emission wavelength is close to 310 $nm$. The image capture system is a 1648 $\times$ 1214 pixels, 12 bit resolution intensified with an average quantum efficiency of 70%. The fluorescence photons crossing the band pass filter (305 $\pm$ 5 $nm$) are focused by the 50 $mm$, F/1.4 Nikon lenses. The intensifier modulates the CCD, decreasing the exposure time from milliseconds to nanoseconds order, for the present set of experiments, a 15 $ns$ gate time was used to capture PLIF-OH images. A pixel corresponds to a bin smaller than 0.1 $mm$ at the measurement plan. The system control and analysis software, DaVis 7.2.2, processes the images interfaced by a 525 KP board, installed at a 32 bit slot in a computer.

The resulting PLIF-OH 2D images are post processed in oder to extract statistical information. The image batch of each combustion regime consisting of $N_s$ samples is post-processed by a digital image processing software, KS400 from Karl Zeiss. The first post processing step consists of a thresholding (binarizing) procedure which zeroes (background) on intensity values below the average and attributes 1 (object) to other intensity values. This allows to obtain well defined flame surfaces which should be limited by surfaces where an equilibrium between species production and diffusion exists. Then, area $S$ and perimeter $P$ of the object are measured in order to yield an estimative of the flame thickness. These parameters are calculated automatically by the software, area is measured integrating the pixels of the object, whereas the perimeter is calculated adding the pixels of the border in object. A dimensionless parameter, $S/P^2$, is supposed to be an estimate of the flame thickness which is important to the flame regime classification process, since it is expected to be affected by the $Da$ and $Re_t$ numbers variations.

## 4. RESULTS AND DISCUSSION

### 4.1 Numerical Predictions

The distribution of the $OH$ radical mass fraction in the mixture fraction $Z$ space for the methane and hydrogen mixtures with air, for different values of scalar dissipation rates $N$, is presented Figure 3. This distribution is obtained from each fuel flamelet library. The maximum value of the $OH$ concentration occurs around the stoichiometry, which corresponds to $Z_{st} = 0.05$ and $Z_{st} = 0.03$ for methane and hydrogen, respectively. This figure shows that the expected $OH$ fluorescence intensity is a factor of 2 higher for $H_2$/air mixtures, when compared to $CH_4$/air flames.

For each fuel air combination, the temperature $T$ is shown as function of mixture fraction $Z$in Figure 4 for different values of scalar dissipation rate $N$. Figures 3 and 4 allows to verify that the maximum value of temperature within the flame is a decreasing function of the scalar dissipation rate, however, the $OH$ mass fraction is a nonmonotonic function of $N$. This precludes a direct link between a local maximum of $OH$ concentration in a direction normal to the flame front and the instantaneous aerodynamical state. Furthermore, Fig. 3 shows that the $OH$ layer thickness, which could be related to a flame thickness, does not exhibit a simple behavior with respect to $N$.

In order to estimate a chemical time scale for each reactant combination, the temperature at stoichiometry is plotted in Figure 5 as function of the scalar dissipation rate $N$. Above a critical value of the scalar dissipation rate ($N^* \cong 11\ s^{-1}$ for $CH_4$ and $N^* \cong 150\ s^{-1}$ for $H_2$) the temperature becomes constant, which means that flame extinction occurs.

The Damköhler versus Reynolds diagram for methane flames obtained numerically from the CFD simulation and from the flamelet library is presented in Figure 6. The flamelet library for methane yields a characteristic chemical timescale of the order $1/11\ s$ that, along with the eddy frequency, was used to determine the Damköhler number.

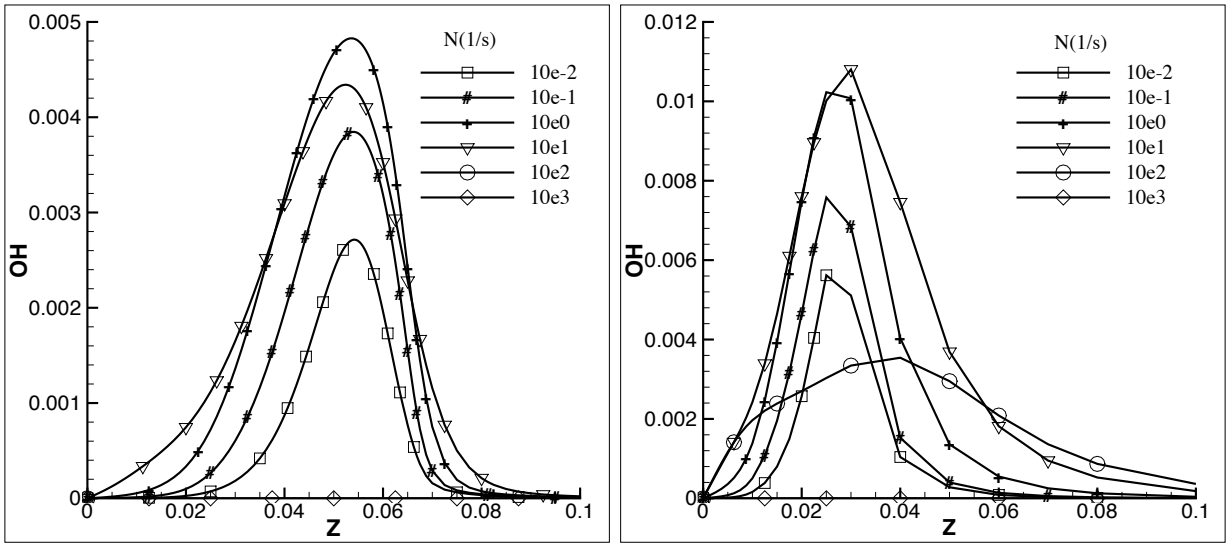


(a) $CH_4$ (b) $H_2$

Figure 3. Mass fraction distribution of the $OH$ radical in the mixture fraction ($Z$) space for different scalar dissipation rates ($N$).

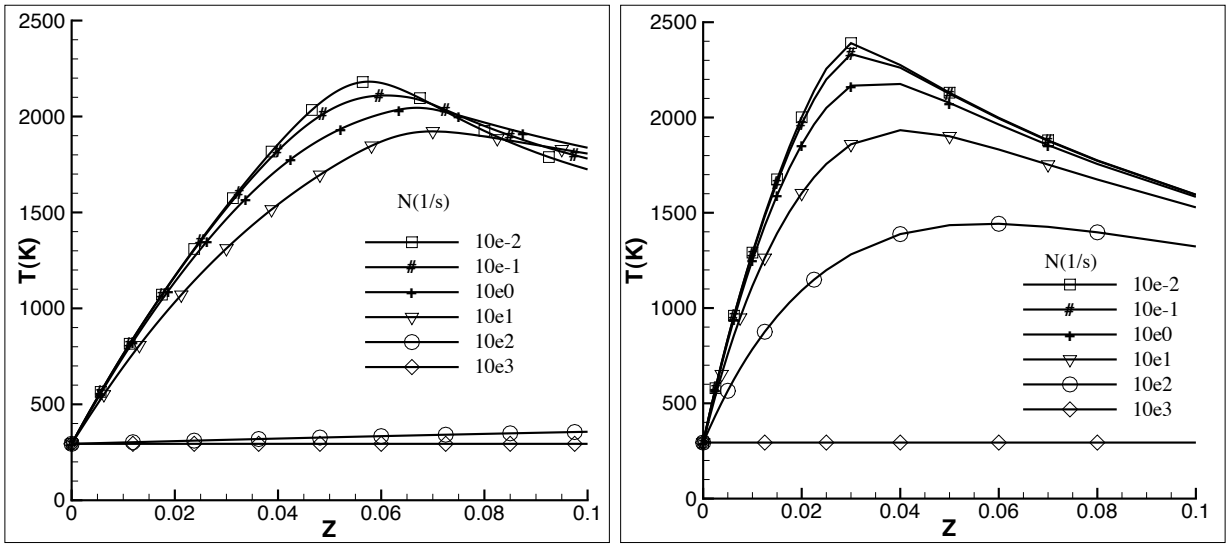


(a) $CH_4$ (b) $H_2$

Figure 4. Distribution of the temperature ($T$) in the mixture fraction ($Z$) space for different scalar dissipation rates ($N$).

This figure depicts the computed combustion regime diagram for methane/air reactants and for the flow conditions listed in Table 1. For the sake of simplicity laminar cases are not shown. It can be clearly seen that the present experimental facility allows to cover a range of turbulent Reynolds numbers between 50 and 3000, and a Damköhler number which spans from 0.1 to 100, thus covering the full range of combustion/turbulence interaction possibilities. The boundaries between the different combustion regimes have been chosen in accordance with the experimental results discussed in the following section.

The hydrogen-air characteristic chemical timescale is of the order $1/150$ $s$, which is an order of magnitude smaller than the timescale of the methane-air combustion. Thus, for a given flow condition, the Damköhler number increases an order of magnitude when the fuel is switched from methane to hydrogen, all else unchanged. This variation in the Damköhler number tends to lead the combustion in the direction of the flamelet regime, as can be seen in Figure 7, where a comparison of the computed regimes for both fuels considered is shown. Therefore, with a given set of flow velocities, one may vary the resulting combustion regime by merely switching fuels.

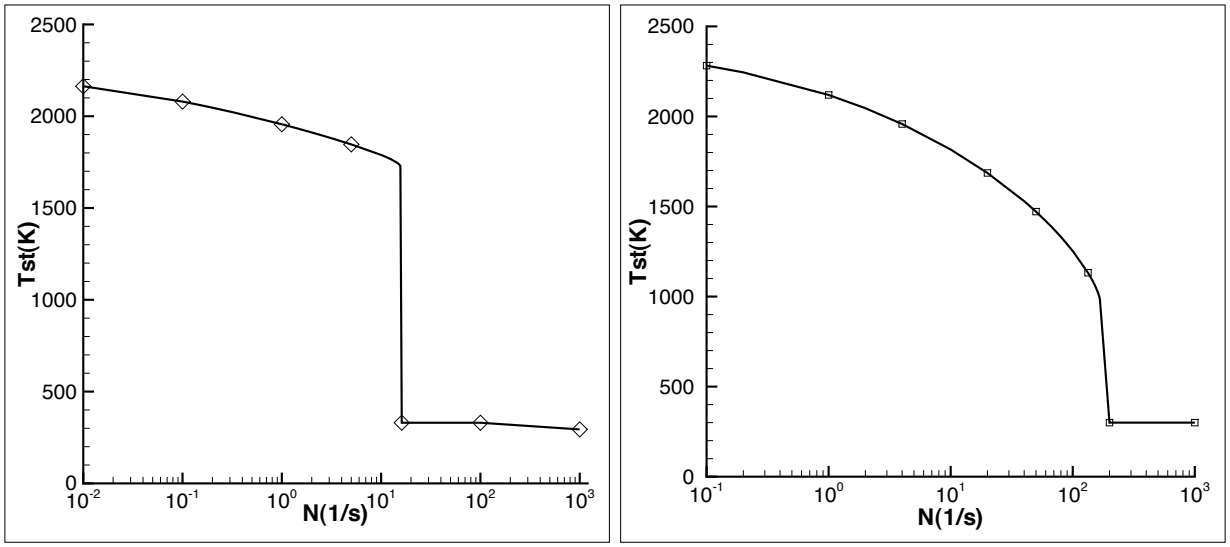


(a) $CH_4$ (b) $H_2$

Figure 5. Temperature at the stoichiometry as a function of scalar dissipation rate ($N$).

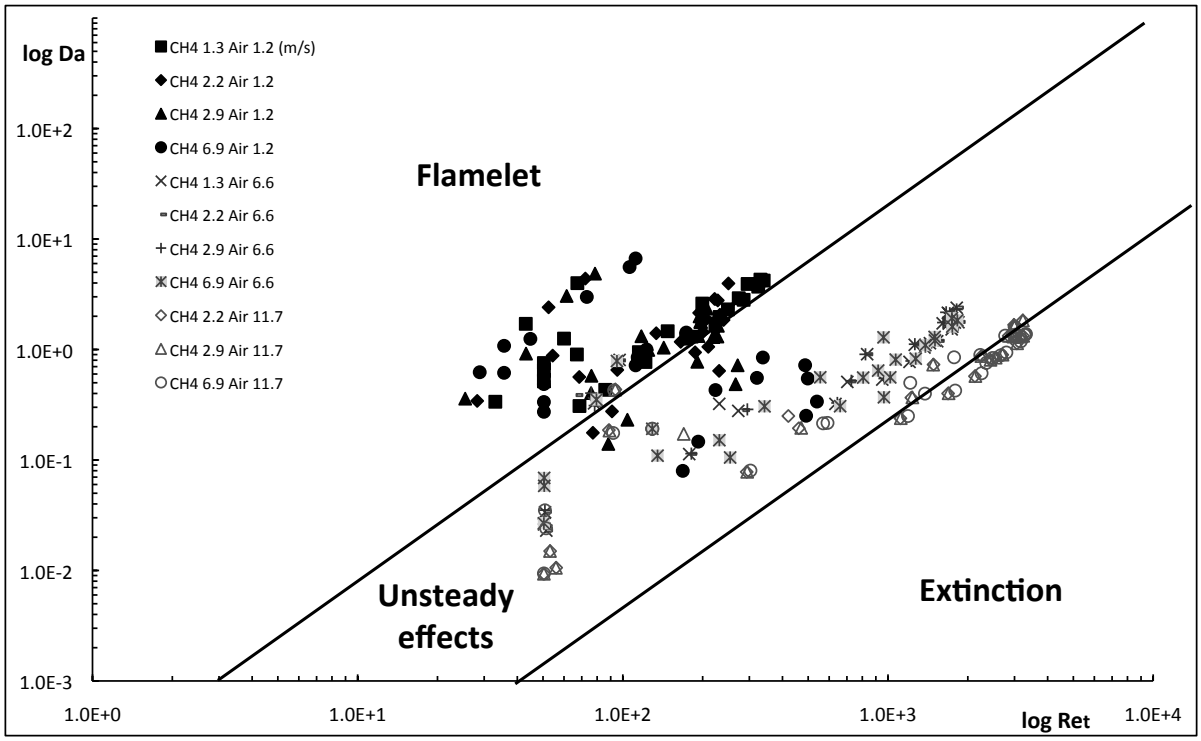


Figure 6. Combustion regimes corresponding to methane air mixtures.

### 4.2 Experimental Results

Combustion diagnostics is performed via a laser technique which consists of capturing images from the $OH$ fluorescence. This radical is supposed to represent the flame front and allows to estimate the flame thickness, which is then analyzed by the image processing. The ratio of the area to square perimeter of the $OH$ signal on each image is determined. This relation is supposed to be a flame thickness estimate, which will be used to quantify changes on the flame structure with the combustion regime.

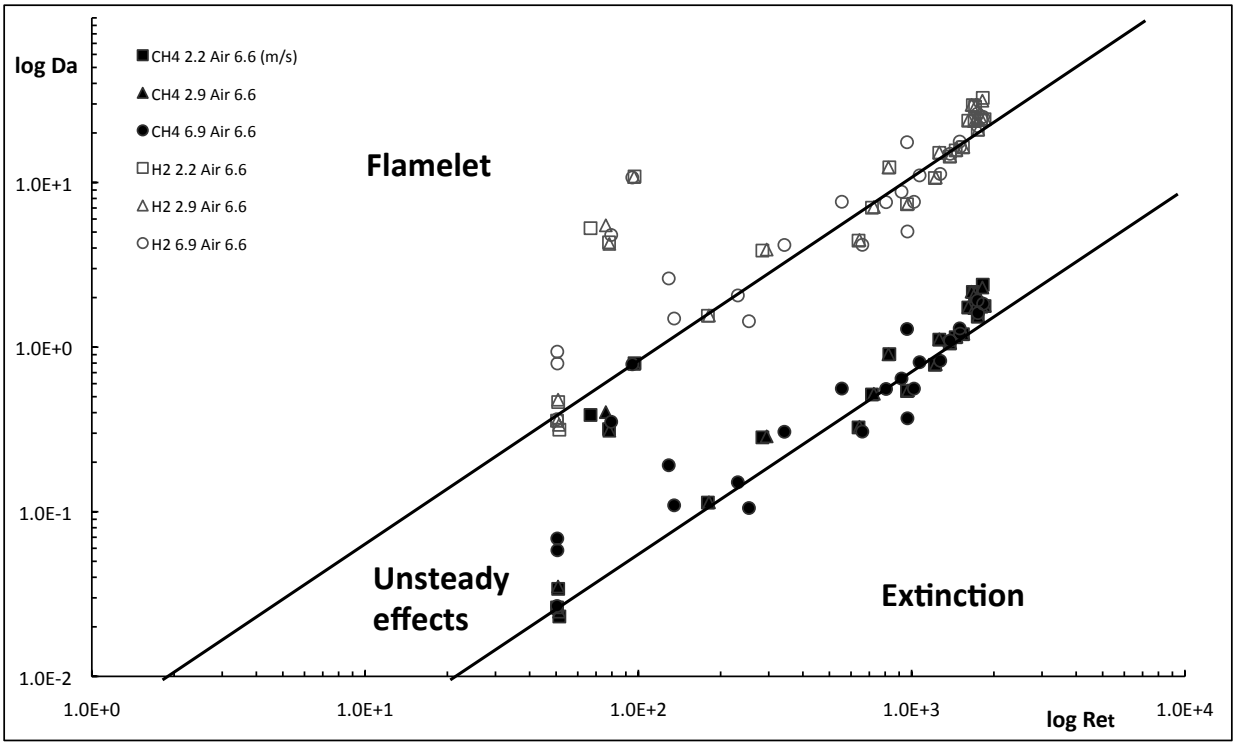


Figure 7. Combustion regimes for methane and hydrogen mixtures with air.

In Figure 8 are shown typical binary instantaneous images of the flames addressed in the natural gas study, which correspond to parameters given in Table 2, namely; volumetric fuel flow rate $\dot{Q}_{fuel}$; fuel jet velocity $U_{fuel}$; Reynolds number based on the fuel feed diameter $Re_D$; the coflow air velocity $U_{air}$; the ratio of the area $S$ by the square of the perimeter $P^2$ of the objects formed by the $OH$ concentration distribution in the PLIF images; a representative turbulent Reynolds number $Re_t$; Damköhler number $Da$ and the flame regime. Figure 9 shows the binary instantaneous images of the flames resulting of the use of hydrogen as fuel and Table 3 contains the corresponding parameters. Note that the flow velocities used in the experiment are not identical to those of the computations.

Table 2. Parameters of each natural gas flame studied.

| *Flame* | $\dot{Q}_{fuel}$ $(Nm^3/h)$ | $U_{fuel}$ $(m/s)$ | $Re_D$ | $U_{air}$ $(m/s)$ | $S/P^2$ $(\times 10^{-2})$ | $Re_t$ | $Da$ | *Regime* |
|---|---|---|---|---|---|---|---|---|
| $M1$ | 0.1 | 0.4 | 150 | 0.0 | 2.1 | — | — | laminar |
| $M2$ | 0.2 | 1.4 | 600 | 1.2 | 3.3 | 3 – 340 | 0 – 4 | flamelet |
| $M3$ | 0.7 | 4.9 | 2100 | 6.6 | 3.4 | 5 – 250 | 0 – 3 | flamelet |
| $M4$ | 0.8 | 5.6 | 2400 | 6.6 | 3.7 | 5 – 250 | 0 – 3 | non flamelet |
| $M5$ | 1.6 | 11.0 | 4800 | 6.6 | 3.6 | 5 – 1800 | 0 – 2 | non flamelet |
| $M6$ | 1.6 | 11.0 | 4800 | 11.7 | 3.8 | 5 – 1800 | 0 – 1 | non flamelet |

The flames $M1$, $H1$ and $H2$ correspond to the laminar regime since they display a stable structure in time, which is verified through the time-average and RMS analysis, not shown here for the sake of brevity. These flames were chosen not to be depicted in the combustion regime diagrams. The flames $M2$, $M3$, $H3$, $H4$, $H5$ and $H6$ belong to the flamelet regime, since the instantaneous behavior exhibits a wrinkled but mostly continuous flame front. The $M4$ flame is at the unsteady effects regime, because it presents local extinctions, air incorporation by the flame front producing small islands non reacting in large and variable thickness, which evidences a low Damköhler number. The $M5$ flame is typical of the the unsteady effects regime, non flamelet, which shows the front flame breaking due to low values of $Da$ and high Reynolds numbers. The $M6$ flame exhibits a reactive zone intermittently blowing off from the burner, presenting local extinctions, wrinkling and broad variations of the instantaneous images from the time-average and RMS. The experimental apparatus does not achieve low values of $Da$ in hydrogen flames so that the unsteady effects regime could be observed.

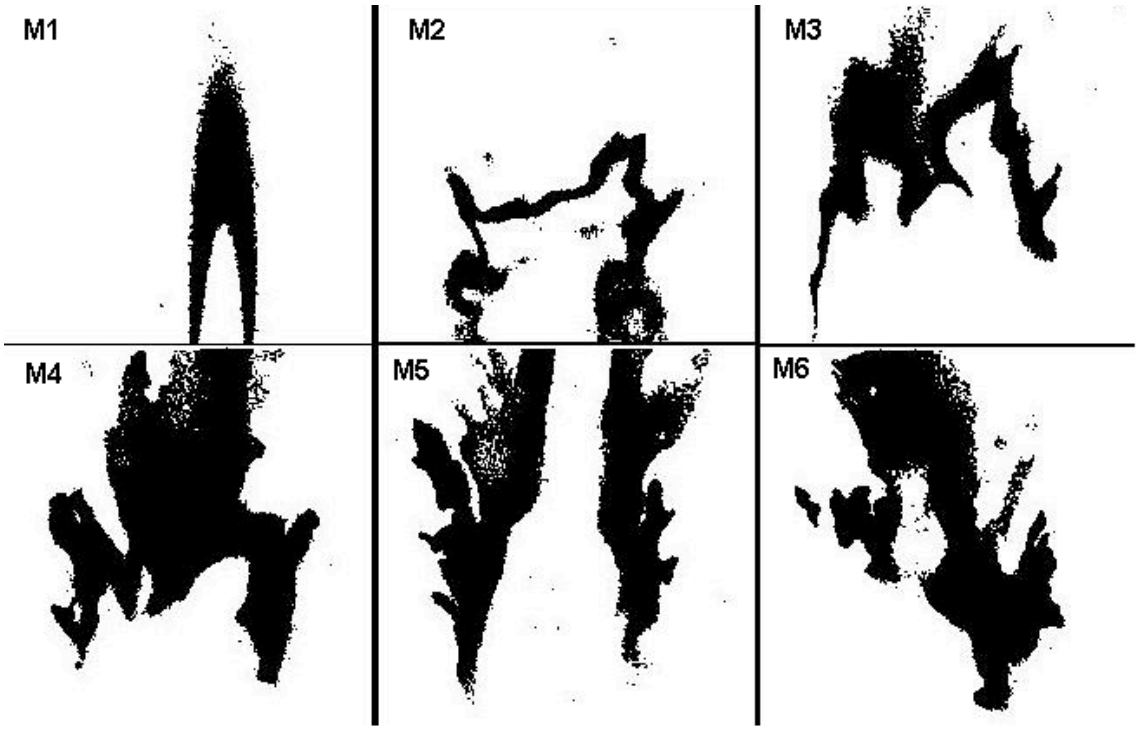


Figure 8. Shifted binary PLIF-OH images of the natural gas flames.

The $S/P^2$ parameter displayed in Tables 2 and 3, which could be used as an estimate of the flame thickness, does not exhibit an obvious correlation with the estimated turbulent Reynolds and Damköhler numbers. The values of $S/P^2$ are higher for turbulent than for laminar flames, but a clear-cut criterium cannot be derived relating this parameter to $Re_t$ or to $Da$.

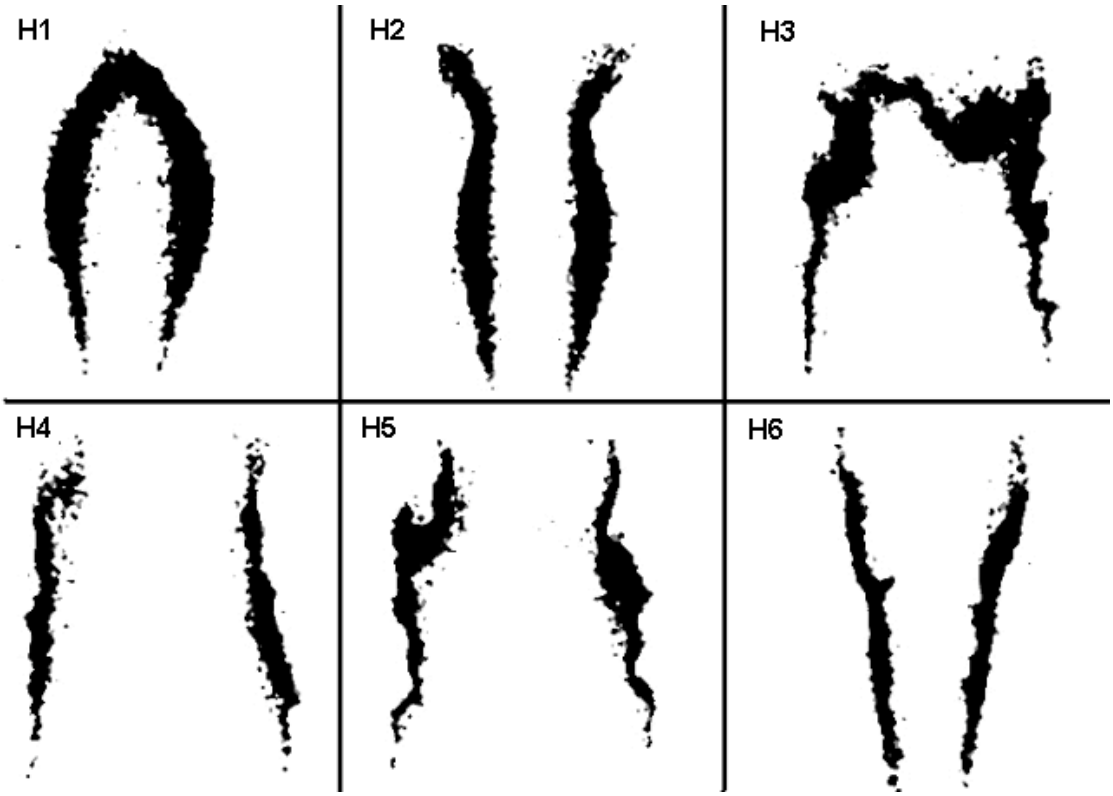


Figure 9. Shifted binary PLIF-OH images of the hydrogen flames.

Table 3. Parameters of each hydrogen flame studied.

| *Flame* | $\dot{Q}_{fuel}$ $(Nm^3/h)$ | $U_{fuel}$ $(m/s)$ | $Re_D$ | $U_{air}$ $(m/s)$ | $S/P^2$ $(\times 10^{-2})$ | $Re_t$ | $Da$ | *Regime* |
|---|---|---|---|---|---|---|---|---|
| $H1$ | 0.7 | 5.0 | 360 | 0.0 | 1.9 | — | — | laminar |
| $H2$ | 4.2 | 30.0 | 2200 | 0.0 | 2.0 | — | — | laminar |
| $H3$ | 1.4 | 9.9 | 730 | 6.6 | 2.9 | 5 – 1800 | 0 – 3 | flamelet |
| $H4$ | 7.1 | 50.0 | 3600 | 0.0 | 3.1 | N/A | N/A | flamelet |
| $H5$ | 4.2 | 30.0 | 2200 | 6.6 | 3.8 | N/A | N/A | flamelet |
| $H6$ | 7.1 | 50.0 | 3600 | 6.6 | 3.0 | N/A | N/A | flamelet |

## 5. CONCLUSIONS AND FUTURE WORKS

This work introduces the characterization results of the natural gas and hydrogen turbulent flames in a situation which the reactants are initially segregated. The bluff-body burner used allows a two order of magnitude variation of turbulent Reynolds and Damköler numbers.

An *a priori* methodology for the numerical determination of the combustion regimes was developed. This kind of analysis is valuable to determine the combustion regimes before the construction of an experimental apparatus or to determine the effects of fuel substitution.

The instantaneous turbulent flame images captured allows the determination of the flame regimes from the information obtained via image processing. The wide variation of the internal structures of the flame front and their discontinuous presence with inter-penetration of the reactants on the combustion absence make the process prediction complex, therefore, the presented results were qualitatively estimated.

A thickness measurements on the PLIF-OH image supplemented by a threshold method aimed at classifying each combustion regime was shown not to be able to classify the flame regime automatically. A flame front curvature analysis should be done in future works in order to determine flame front wrinkling.

Future work should be devoted to improving the current experimental analysis methods by performing simultaneous velocity/scalar measurements. Such measures would allow the development of more refined regime identification techniques than those introduced here. Furthermore, comparisons between the experimental results and modelled reactive flows should be performed in order to assess the predictive capability of these models.

## 6. ACKNOWLEDGMENTS

This work was performed while the forth author was a Visiting Professor, funded by the Brazilian Petroleum Agency (ANP), on leave from Centre National de la Recherche Scientifique, France. The authors acknowledge the support awarded to this research from the Brazilian Council for Scientific and Technological Development (CNPq), Rio de Janeiro State Scientific Foundation (FAPERJ) and Petróleo Brasileiro S/A (Petrobras). They are also grateful to Jonhatan Lemay (Université du Québec) for the bluff-body geometry and mesh; Elder Marino Mendoza Orbegoso (PUC–Rio) for the help with the modified OPPDIF code; Luis Enrique Alva Huapaya (PUC–Rio) for the detailed information about bluff-body experiment; and Amanda Gloria Santos da Cunha for the bluff-body sketch.

## 7. REFERENCES

Alva, L. E. (2008). Numerical and Experimental Characterization of a Non-Premixed Turbulent Flame. M.Sc. Dissertation, Pontifícia Universidade Católica do Rio de Janeiro, Rio de Janeiro. (in Portuguese).

Alva, L. E., Figueira da Silva, L. F., and Azevedo, L. F. A. (2008). Numerical and experimental characterization of a non-premixed turbulent flame. In *Proceedings of ENCIT 2008*.

Alvarez Aquino, M. A. (2006). Development of a Natural Gas Burner for the Studies of Combustion in Turbulent Flows. M.Sc. Dissertation, Pontifícia Universidade Católica do Rio de Janeiro, Rio de Janeiro. (in Portuguese).

Alvarez Aquino, M. A., Figueira da Silva, L. F., and Azevedo, L. F. A. (2007). Non-reactive flowfield characterization of a natural gas burner for turbulent combustion studies. In *Proceedings of COBEM 2007*.

Bowman, C., Hanson, R., Davidson, D., W.C. Gardiner, J., Lissianski, V., Smith, G., Golden, D., Frenklach, M., and Goldenberg, M. (1998). GRI-Mech 2.11. Technical Report, Gas Research Institute. `http://www.me.berkeley.edu/gri_mech/`.

Dally, B. B., Masri, A. R., Barlow, R. S., and Fiechtner, G. J. (1998). Instantaneous and mean compositional structure of bluff-body stabilized nonpremixed flames. *Combustion and Flame*, Vol. 114, No. 1-2, pp. 119–148. doi:10.1016/S0010-2180(97)00280-0.

Dally, B. B., Masri, A. R., Barlow, R. S., and Fiechtner, G. J. (2003). Two-photon laser-induced fluorescence measurement of CO in turbulent non-premixed bluff body flames. *Combustion and Flame*, Vol. 132, No. 1-2, pp. 272–274. doi:10.1016/S0010-2180(97)00280-0.

Jones, W. and Launder, B. (1972). The prediction of laminarization with a two-equation model of turbulence. *International Journal of Heat and Mass Transfer*, Vol. 15, No. 2, pp. 301–314. doi:10.1016/0017-9310(72)90076-2.

Kee, R. J., Rupley, F. M., and Miller, J. A. (1989). CHEMKIN-II: A Fortran Chemical Kinetics Package for the Analysis of Gas-Phase Chemical Kinetics. Technical Report SAND 89-8009, Sandia National Laboratories, Livermore.

Lemay, J., Figueira da Silva, L. F., and Seers, P. (2008). Comparisons of turbulence models in a non-premixed combustion situation. In *32nd International Symposium on Combustion*. Work in Progress Poster.

Li, J., Zhao, Z., Kazakov, A., and Dryer, F. L. (2004). An updated comprehensive kinetic model of hydrogen combustion. *International Journal of Chemical Kinetics*, Vol. 36, No. 10, pp. 566–575. doi:10.1002/kin.20026.

Lutz, A. E., Kee, R. J., Grcar, J. F., and Rupley, F. M. (1996). OPPDIF: A Fortran Program for Computing Opposed-Flow Diffusion Flames. Technical Report SAND 96-8243, Sandia National Laboratories, Livermore.

Merci, B., Dick, E., Vierendeels, J., Roekaerts, D., and Peeters, T. W. J. (2001). Application of a new cubic turbulence model to piloted and bluff-body diffusion flames. *Combustion and Flame*, Vol. 126, No. 1-2, pp. 1533–1556. doi:10.1016/0017-9310(72)90076-2.

Petersson, P., Olofsson, J., Brackman, C., Seyfried, H., Zetterberg, J., Richter, M., Aldén, M., Linne, M. A., Cheng, R. K., Nauert, A., Geyer, D., and Dreizler, A. (2007). Simultaneous PIV/OH-PLIF, Rayleigh thermometry/OH-PLIF and stereo PIV measurements in a low-swirl flame. *Applied Optics*, Vol. 46, No. 19, pp. 3928–3936. doi:10.1364/AO.46.003928.

Poinsot, T. and Veynante, D. (2005). *Theoretical and Numerical Combustion*. Edwards, Philadelphia, 2nd edition.

Wolfrum, J. (1998). Lasers in combustion: From basic theory to practical devices. *Symposium (International) on Combustion*, Vol. 27, No. 1, pp. 1–41. doi:10.1016/S0082-0784(98)80387-1.